Estimating fatigue damage in a CFRP laminate with a hole using an embedded FBG sensor

S. Yashiro[1], T. Okabe[2]
[1]*Ehime University, Matsuyama, Japan;*
[2]*Tohoku University, Sendai, Japan;*
E-mail: *yashiro@eng.ehime-u.ac.jp*

1. Introduction

Carbon fiber reinforced plastics (CFRPs) have frequently been applied to various structures because of their light weight, high strength and modulus, and superior fatigue properties. Damage accumulates in composite structures due to cyclic loading; stress concentrations induce complex damage states that include ply cracks and delamination. The accumulation of damage causes the loss of structural stability and also becomes the source of damage extension. Accordingly, nondestructive testing systems have been used to ensure structural reliability. However, current inspection techniques involve complex procedures, which can be very labor-intensive and expensive.

Structural health-monitoring (SHM), which constantly inspects the condition, has been intensely investigated to overcome these difficulties. Among various SHM techniques, fiber-optic-based methods have attracted attention because of their small sensor size, high sensitivity and no electric/magnetic induction. Fiber Bragg grating (FBG) sensors have the advantages such as high-accuracy for strain or temperature measurement. Furthermore, FBG sensors have high-sensitivity to non-uniform strain distributions, and this characteristic was utilized for detecting damage in CFRP laminates [1].

The authors [2] demonstrated that the spectrum of reflected light from an embedded FBG sensor was useful for monitoring the damage process in notched CFRP laminates. Moreover, we [3] proposed an inverse method to identify the damage based on the reflection spectrum of an embedded FBG sensor, and successfully predicted the damage pattern observed in a static tensile test for a notched laminate. In order to demonstrate the usefulness of this technique in engineering problems, fatigue damage should be evaluated by using the embedded FBG sensor.

In the present study, we conducted tensile fatigue tests for holed CFRP cross-ply laminates with an embedded FBG sensor, and experimentally investigated the change in the reflection spectrum of the FBG sensor. Then, the mechanism for detecting damage by the embedded FBG sensor was considered. Furthermore, this study also numerically predicted the damage pattern near the hole based on the sensor signal measured in the experiment.

2. Experiment procedure

A cross-ply laminate was fabricated by using CFRP prepreg sheets (T800H/#3631, Toray Industries); the stacking configuration was $[0_2/90_2]_S$. Before fabrication, we embedded an FBG sensor (NTT-AT) in a 0° ply along the direction of reinforcing fibers. Figure 1 presents the dimensions of the specimen. The specimen coupon was 180 mm long, 30 mm wide and 1 mm thick; the radius of the hole was 5 mm. GFRP tabs were glued at the ends of the specimen.

The gage length of the FBG sensor was 10 mm, and one end of the gage section was located nearest to the hole edge (Fig. 1). The distance between the hole edge and the end of the gage section was 1.0 mm. The FBG sensor was embedded in contact with 90° plies to improve the sensitivity to various damage types. The FBG sensor was coated with polyimide resin; the outside diameter was 150 μm.

The refractive index of the core in an optical fiber periodically changes along the gage section of an FBG sensor; this index change is known as grating. When the optical fiber is illuminated by broadband light, a narrowband component is reflected from the gratings. The wavelength of the reflection λ is specified by the grating period Λ as $\lambda = 2n\Lambda$ (n: effective refractive index of the core). Then, the wavelength (spectrum) of the reflection can measure the strain (strain distribution) in the gage section, since the grating period and the refractive index changes with the longitudinal strain [1].

Tensile fatigue tests were conducted at room temperature with a sinusoidal waveform under load control conditions by using a servo-hydraulic controlled testing machine (INSTRON 8516). The maximum stress was 336 MPa with the stress ratio R = 0.14; the test speed was 5 Hz. The reflection spectrum was measured after predetermined loading cycles by an optical spectrum analyzer (AQ6319, Ando Electric) with a broadband light source (AQ4315A, Ando Electric). The specimens then observed by soft X-ray radiography.

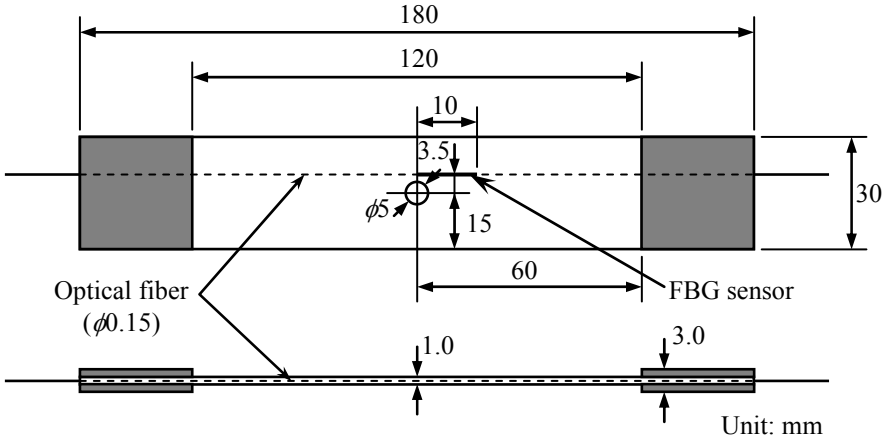

Fig. 1 Dimensions of a CFRP specimen with an open hole. An optical fiber with an FBG sensor was embedded in the 0° ply in contact with the 90° plies.

3. Damage identification procedure

3.1 Finite-element model

This study analyzed the strain distribution in a cross-ply laminate with a hole by a layer-wise finite-element model with cohesive elements [2]. Figure 2 depicts the finite-element model for the laminate with the embedded optical fiber, considering the symmetry for the through-thickness direction. The dimensions were 15 mm in the longitudinal (x) direction and 15 mm in the transverse (y) direction. The model was separated into two layers of 0° plies and 90° plies to express the stacking configuration of $[0/90]_S$. Both layers were 0.25 mm thick, and four-node Mindlin plate elements were applied to these layers to address an out-of-plane deformation. An optical fiber was also built into the 0° layer as two-node truss elements. The edge along the x-direction was loaded by a uniform tensile displacement. The thermal residual stresses due to the temperature change in the curing process, $\Delta T = -160$ K, were also considered. Table 1 lists the material properties used in the analysis.

Three types of damage (i.e., splits, transverse cracks, and delamination) were expressed by cohesive elements as illustrated in Fig. 2. Cohesive elements for splits were located in the 0° layer from the edge of the hole along the longitudinal (x) direction. Transverse cracks were expressed by the cohesive elements in the 90° layer at equal intervals of crack spacing. Finally, cohesive elements for delamination were inserted into all 0°/90° layer interfaces.

We used the cohesive elements proposed by Geubelle et al. [4]. This element exhibited a bi-linear relation between the traction and the relative displacement of plate elements and easily calculated mixed-mode cracking. The relation between the traction T and the relative displacement Δ was defined by using the parameter s as

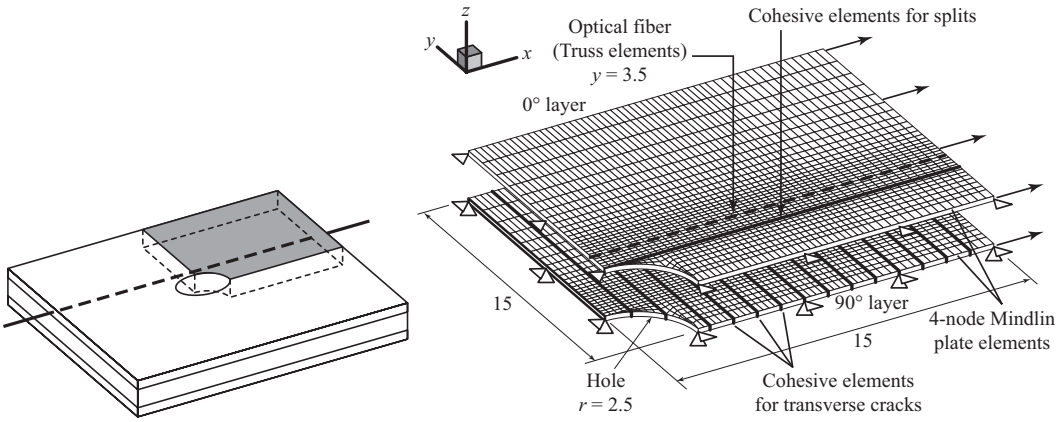

(a) Schematic (b) Finite-element model

Fig. 2 Layer-wise finite-element model with cohesive elements for a holed cross-ply laminate with an embedded optical fiber.

Table 1 Material properties of the CFRP laminate.

Longitudinal Young's modulus (GPa)	148
Transverse Young's modulus (GPa)	9.6
In-plane shear modulus (GPa)	4.5
Out-of-plane shear modulus (GPa)	3.5
In-plane Poisson's ratio	0.36
Out-of-plane Poisson's ratio	0.49
Longitudinal thermal expansion coef. (x10^{-6}/)	-0.6
Transverse thermal expansion coef. (x10^{-6}/K)	36

Table 2 Properties of cohesive elements.

	Ply cracks	Delamination
In-plane tensile strength (MPa)	84	40
In-plane shear strength (MPa)	100	60
Out-of-plane shear strength (MPa)	100	60
Mode I critical energy release rate (J/m^2)	310	500
Mode II critical energy release rate (J/m^2)	600	700
Mode III critical energy release rate (J/m^2)	600	700

$$T_i = \frac{s}{1-s}\frac{\Delta_i}{\Delta_{i\mathrm{c}}}\tau_{i\max} \qquad (i = \mathrm{n, t, b}), \tag{1}$$

$$\Delta_{\mathrm{nc}} = \frac{2G_{\mathrm{Ic}}}{\tau_{\mathrm{n}\max} s_{\mathrm{ini}}},\ \Delta_{\mathrm{tc}} = \frac{2G_{\mathrm{IIc}}}{\tau_{\mathrm{t}\max} s_{\mathrm{ini}}},\ \Delta_{\mathrm{bc}} = \frac{2G_{\mathrm{IIIc}}}{\tau_{\mathrm{b}\max} s_{\mathrm{ini}}}, \tag{2}$$

where $\tau_{i\max}$ is the maximum stress and Δ_{ic} (i = n, t, b) is the critical relative displacement; the subscripts n, t, and b indicate the cracking modes of normal tension, in-plane shear, and out-of-plane shear. The critical relative displacement when the element completely lost traction, Eq. (2), was defined by the energy criterion: G_{ic} (i = I, II, III) is the critical energy release rate, and s_{ini} (=0.999 in this study) is the initial value of the parameter s.

This cohesive element acts as a penalty element during $s = s_{\mathrm{ini}}$ with small relative displacement, and generates a crack surface that yield no traction if s = 0. Equation (1) indicates that the parameter s represents the residual strength of the element. Table 2 lists the properties of cohesive elements.

3.2 Optical analysis

The refractive index of the core changes periodically in an FBG sensor. Reverse mode coupling then occurs in the same waveguide. The reflection spectrum can be calculated by analyzing this mode coupling between the forward (incident) light and the backward (reflected) light. A detailed description of the calculation method for a reflection spectrum can be found in the other papers [3,5].

The FBG sensor embedded in the laminate had a strain distribution along the gage section due to the stress concentration and the damage. The strain distribution greatly affected the reflection spectrum through the grating period Λ and the effective refractive index of the fiber core n_{eff}. The distributions of these two parameters were obtained in terms of the longitudinal strain distribution $\varepsilon_{\mathrm{f}}(x)$ as

$$\Lambda(x) = \left\{1 + \varepsilon_{\mathrm{f}}(x)\right\}\Lambda_0, \tag{3}$$

$$n_{\mathrm{eff}}(x) = n_0 - \frac{n_0^3}{2}\left\{p_{12} - \nu_{\mathrm{f}}\left(p_{11} + p_{12}\right)\right\}\varepsilon_{\mathrm{f}}(x). \tag{4}$$

Here, Λ_0 is the initial grating period, and p_{11} and p_{12} are the Pockel constants where indices 1 and 2 indicate the axial and transverse directions of the optical fiber. The gage section was located at $0 \le x \le 10$, y = 3.5 in the finite-element model. Table 3 provides the optical properties used in the analysis.

Table 3 Parameters of the optical fiber and the FBG sensor.

Initial center wavelength λ_0 (nm)	1555.0	Strain-optic coefficient p_{11}	0.113
Initial refractive index of the core n_0	1.4490	Strain-optic coefficient p_{12}	0.252

3.3 Damage identification

The damage pattern near the hole was estimated from the measured reflection spectrum by using the inverse method proposed by the authors [3]. This method used an optimization technique; the reflection spectrum obtained by the analysis was fitted to the measured one as a function of the damage pattern represented by some variables.

The estimation of the damage pattern is defined as an optimization problem that minimizes the square errors F_0 between the measured spectrum and the temporarily-estimated spectrum.

$$\text{Minimize}: \quad F_0(\mathbf{d}) = \sum_{m=0}^{100} \{a_m - \tilde{a}_m(\mathbf{d})\}^2 \tag{5}$$

Design variables: **d**

We represented the reflection spectrum by Fourier series to evaluate the spectrum shape quantitatively; the variables a_m and $\tilde{a}_m$ are the mth Fourier coefficient for the input and the estimated spectra. The Fourier coefficients under 100th order are used in Eq. (5). The components of the vector **d** are design variables that correspond to the damage near the hole. The damage pattern is expressed in the finite-element model by controlling the distribution of the residual strength parameter s of the cohesive elements as functions of the design variables.

Figure 3 illustrates a definition of the design variables (components of the vector **d**). The delaminated region is approximated by the following equation using the Cartesian coordinates ξ–η whose origin is located at $(x, y) = (2.0, 2.5)$.

$$\left(\frac{\xi}{d_{\mathrm{d1}}}\right)^{\alpha} + \left(\frac{\eta}{d_{\mathrm{d2}}}\right)^{\beta} \le 1, \quad \xi \ge 0, \ \eta \ge 0 \tag{6}$$

The variables d_{d1} and d_{d2} express the size of the delamination in the longitudinal direction and the transverse direction, and the variables α and β defines the delamination shape. The residual strength parameter s of the cohesive elements was zero in the delaminated region.

We also represent the damage process zone ($0 < s < s_{\mathrm{ini}}$) of the delamination by the length d_{d3} in the longitudinal direction. Here, the shape of the delamination process zone is assumed to be the same as the perfectly delaminated zone. The distribution of the residual strength in the delamination process zone is expressed as a parabolic function of distance r from the origin of the ξ–η coordinates.

$$s = s_{\mathrm{ini}} r^p, \quad 0 \le r \le 1 \tag{7}$$

The variable p defines the decrease of the residual strength, where r is normalized by the length of the process zone, as indicated in Fig. 3(a).

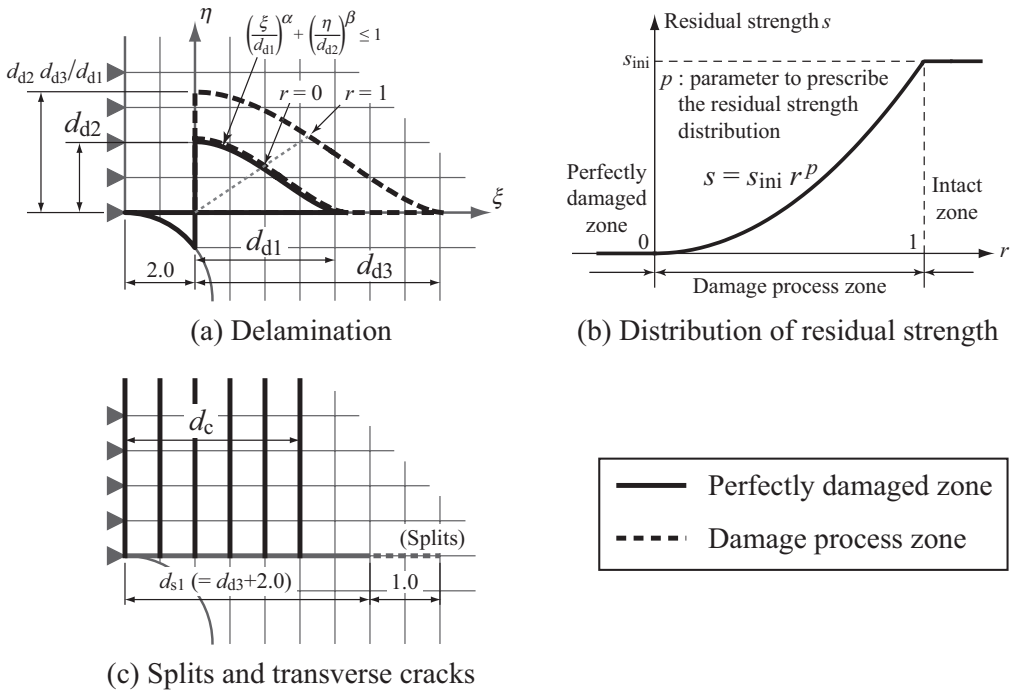

Fig. 3 Definition of the design variables to represent the damage pattern.

The variable d_c represents the region where transverse cracks are generated in the 90° plies; these transverse cracks are assumed to penetrate the ligament area. Splits have minimal effect on the embedded FBG sensor parallel to the fiber direction [2,6]. The lengths of the split and the splitting process zone are then related to the size of the delamination process zone (d_{d3}), since the extension of the splits causes delamination. Consequently, the damage pattern near the hole is represented by these seven design variables, i.e., $\mathbf{d} = \{d_{d1}, d_{d2}, d_{d3}, \alpha, \beta, p, d_c\}^T$.

These variables are optimized by Fletcher and Powell method for minimizing the objective function $F_0(\mathbf{d})$, and the golden-section method is adopted as the linear search method. We also apply tunneling algorithm [7] to the global minimization since the objective function contains many local minimum points.

4. Results and discussion

4.1 Experiment results

Figure 4 presents the soft X-ray photographs of damage patterns in the holed specimens at some loading cycles. We observed splits in the 0° plies, transverse cracks in 90° plies, and delamination at the 0°/90° ply interfaces near the hole. First, small splits and transverse cracks were generated from the hole edge at the early stage of cyclic loading. The splits extended along the fiber direction, and more transverse cracks appeared with increasing number of cycles. These transverse cracks initially had small length and then grew to penetrate the ligament area. Delamination was initiated and extended in a quarter-elliptical shape along the splits after some extension of the ply cracks.

Figure 5 illustrates the reflection spectra of the FBG sensor at some numbers of cycles; these spectra were measured at the mean stress level. First, the spectrum became broad because of the longitudinal strain distribution in the gage section

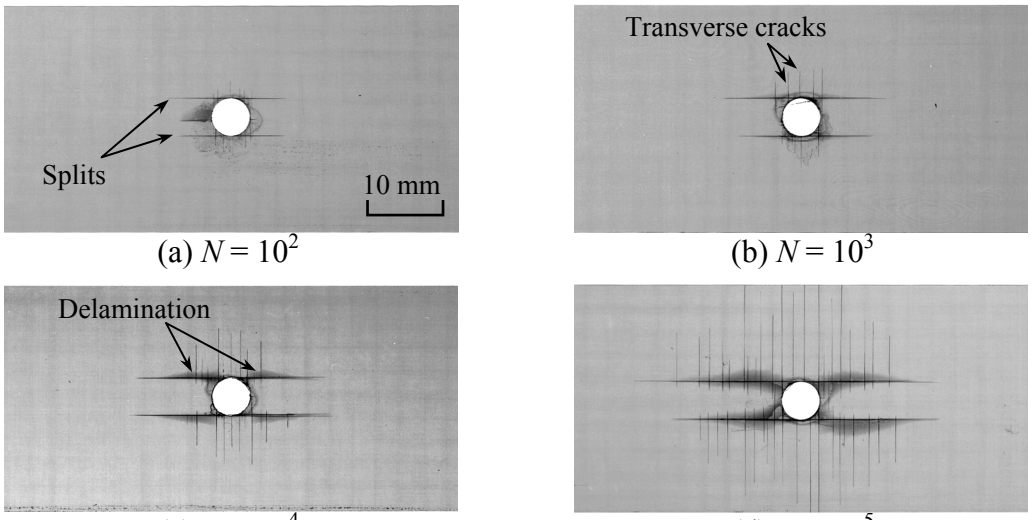

(a) $N = 10^2$ (b) $N = 10^3$

(c) $N = 10^4$ (d) $N = 10^5$

Fig. 4 X-ray photographs of CFRP cross-ply laminates with a hole.

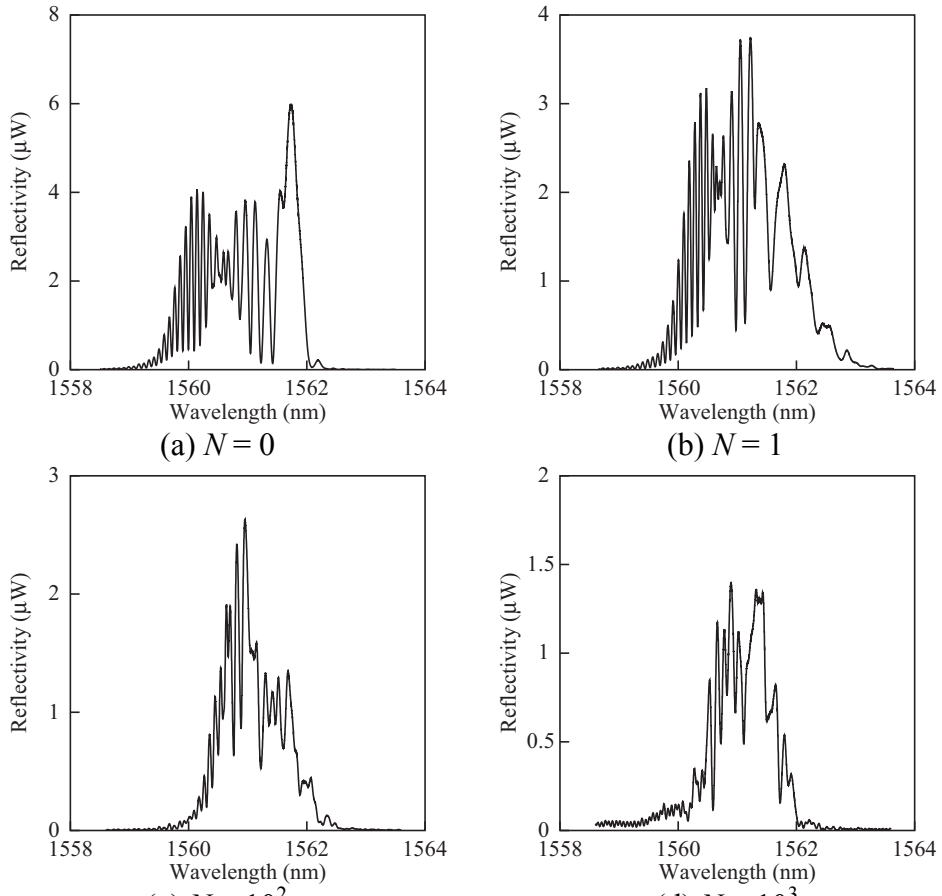

(a) $N = 0$ (b) $N = 1$

(c) $N = 10^2$ (d) $N = 10^3$

Fig. 5 Reflection spectra measured under the mean stress condition.

induced by the stress concentration of the hole (Fig. 5(a)). The shape of the spectrum gradually changed with increasing number of cycles, and the spectrum shifted slightly to a longer wavelength, despite the same applied stress. The damage extension depicted in Fig. 4 caused these changes in the reflection spectrum; the spectrum width became small again by the delamination, since the delamination near the hole produced almost constant and high strain in the gage section [6]. Thus, the damage extension near the hole could be detected by the embedded FBG sensor.

4.2 Damage identification

The damage pattern near the hole in a cross-ply laminate was estimated from the reflection spectrum measured under the mean-stress condition at number of cycles $N = 10^3$ (Fig. 5(d)). Figure 6(a) compares the measured spectrum with the reproduced spectrum, where these spectra were normalized by the maximum reflectivity. The obtained spectrum had several peaks within the shorter wavelengths (1560.5-1561.5 nm) and one large peak at 1561.5 nm; the inverse method produced a similar spectrum shape to the experimental one.

Figure 6(b) depicts the estimated damage pattern at $N = 10^3$. The small delamination size in the longitudinal direction was identified well even though transverse cracks were overestimated compared to the observation (Fig. 4(b)). This result indicated that the delamination had greater sensitivity to the spectrum shape than to transverse cracks. The delamination size in the transverse direction was also overestimated. This error resulted from the low sensitivity of the FBG sensor in the direction normal to itself, and additional sensor embedding could improve the accuracy in the delamination size.

The same damage pattern was also estimated from the spectrum measured under the stress-free condition (Fig. 7(a) solid line). The reflection spectrum initially had a narrow peak with band-width of 0.25 nm before fabrication. Although the spectrum became slightly broad after fabrication due to the birefringence effect induced by the thermal residual stresses, the spectrum still had one peak. The spectrum shape at stress-free condition also changed from the one before the fatigue test. The embedded FBG sensor was subjected to the thermal residual strain of the laminate, and the distribution of the residual strain changed with the damage extension. Therefore, the deformed spectrum shape indicated the thermal residual stress distribution distorted by the damage.

The dashed line in Fig. 7(a) illustrates the estimated spectrum at the stress-free condition. In this case, almost one large peak was obtained, and the spectrum width in the estimation coincided with the measured one. However, the measured spectrum exhibited rugged shape in the large peak. The estimated damage pattern is then depicted in Fig. 7(b). The estimated damage pattern with almost no delamination and the many transverse cracks did not coincide with the observation depicted in Fig. 4(b).

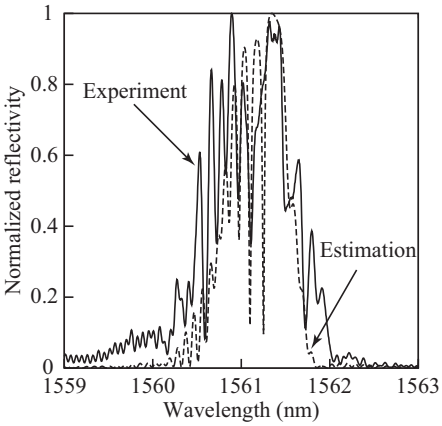

(a) Reflection spectrum

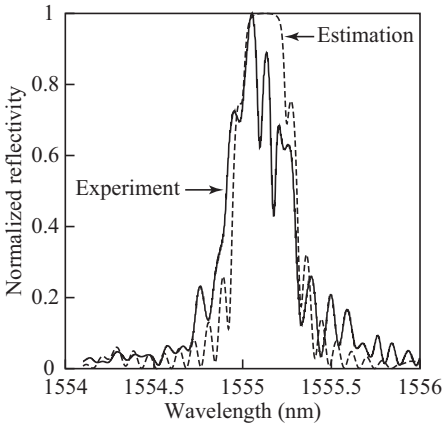

(a) Reflection spectrum

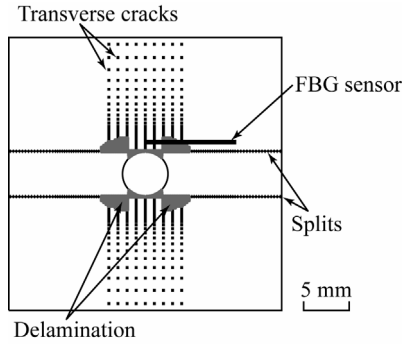

(b) Estimated damage pattern

Fig. 6 Estimated results for the experiment results at N=10^3 from the reflection spectrum measured under the mean stress condition.

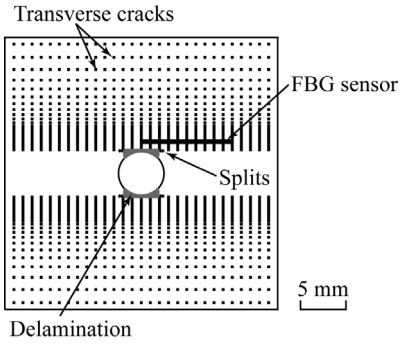

(b) Estimated damage pattern

Fig. 7 Estimated results for the experiment results at N=10^3 from the reflection spectrum measured under the stress-free condition.

The grating period became almost constant in the gage section, and the reflection spectrum had one narrow peak when the specimen was completely unloaded, since the effect of the stress concentration was diminished. Then, one-to-one correspondence between the position in the gage section (i.e., the location of damage) and the wavelength in the reflection spectrum disappeared. Consequently, the spectrum shape lost the one-to-one correspondence to the damage pattern. In this case, a special FBG sensor with an initially chirped grating structure [6] was necessary to identify the damage.

5. Conclusions

This study investigated damage identification in a holed CFRP cross-ply laminate by using an embedded FBG sensor. To this end, we experimentally observed the change in the reflection spectrum from the FBG sensor during the fatigue test. The observed damage pattern near the hole was then numerically estimated from the reflection spectra measured under loaded and unloaded conditions. The conclusions are summarized below.

(1) Splits, transverse cracks and delamination extended near the hole during the fatigue test. The damage extension caused the change in the shape of the reflection spectrum from the embedded FBG sensor. The spectrum shape measured under the stress-free condition was also deformed due to the distribution of the thermal residual stress distorted by the damage.

(2) The estimated damage pattern agreed with the observation when the reflection spectrum measured under the mean stress condition was used as the input information. However, poor prediction was obtained from the reflection spectrum measured under the stress-free condition, since the gradual change in the grating period along the gage section disappeared by unloading.

Acknowledgement

One author (S. Y.) acknowledges support from the Mazda Foundation under a research grant.

References

[1] Y. Okabe, S. Yashiro, T. Kosaka, N. Takeda, Detection of transverse cracks in CFRP composites using embedded fiber Bragg grating sensors, Smart Mater Struct 9 (6) (2000) 832-838
[2] S. Yashiro, T. Okabe, N. Takeda, H. Sekine, A new approach to predicting multiple damage states in composite laminates with embedded FBG sensors, Compos Sci Technol 65 (3-4) (2005) 659-667
[3] N. Takeda, S. Yashiro, T. Okabe, Estimation of the damage patterns in notched laminates with embedded FBG sensors, Compos Sci Technol 66 (5) (2006) 684-693
[4] P.H. Geubelle, J.S. Baylor, Impact-induced delamination of composites: a 2D simulation, Compos Part B 29 (5) (1998) 589-602
[5] S. Huang, M. LeBlanc, M.M. Ohn, R.M. Measures, Bragg intragrating structural sensing, Applied Optics 34 (22) (1995) 5003-5009
[6] S. Yashiro, T. Okabe, N. Toyama, N. Takeda, Monitoring damage in holed CFRP laminates using embedded chirped FBG sensors, Int J Solits Struct 44 (2) (2007) 603-613
[7] A.V. Levy, A. Montalvo, The tunneling algorithm for the global minimization of functions, SIAM J Sci Comput 6 (1) (1985) 15-29